Agricultural and Forest Meteorology 308–309 (2021) 108558

Contents lists available at ScienceDirect

Agricultural and Forest Meteorology

journal homepage: www.elsevier.com/locate/agrformet

Crop yield forecasting and associated optimum lead time analysis based on multi-source environmental data across China

Linchao Li [a,b,c], Bin Wang [b,d], Puyu Feng [e], Huanhuan Wang [a,b], Qinsi He [b,f], Yakai Wang [a,b], De Li Liu [d,g], Yi Li [h], Jianqiang He [h], Hao Feng [b,h], Guijun Yang [c,*], Qiang Yu [b,f,i,*]

[a] College of Natural Resources and Environment, Northwest A&F University, Yangling 712100, China
[b] State Key Laboratory of Soil Erosion and Dryland Farming on the Loess Plateau, Institute of Soil and Water Conservation, Northwest A&F University, Yangling 712100, China
[c] Key Laboratory of Quantitative Remote Sensing in Agriculture, Ministry of Agriculture and Rural Affairs, Beijing Research Center for Information Technology in Agriculture, Beijing 100097, China
[d] NSW Department of Primary Industries, Wagga Wagga Agricultural Institute, Wagga Wagga, NSW 2650, Australia
[e] College of Land Science and Technology, China Agricultural University, Beijing 100193, China
[f] School of Life Sciences, Faculty of Science, University of Technology Sydney, PO Box 123, Broadway, NSW 2007, Australia
[g] Climate Change Research Centre, University of New South Wales, Sydney, NSW 2052, Australia
[h] College of Water Resources and Architectural Engineering, Northwest A&F University, Yangling, 712100, China
[i] Key Laboratory of Water Cycle and Related Land Surface Processes, Institute of Geographic Sciences and Natural Resources Research, Chinese Academy of Sciences, Beijing 100101, China

A R T I C L E I N F O

Keywords:
Crop yield forecast
Climate extremes
Remote sensing
Random forest
Lead time
Variable importance

A B S T R A C T

Accurate and timely crop yield forecasts can provide essential information to make conclusive agricultural policies and to conduct investments. Recent studies have used different machine learning techniques to develop such yield forecast systems for single crops at regional scales. However, no study has used multiple sources of environmental predictors (climate, soil, and vegetation) to forecast yields for three major crops in China. In this study, we adopted 7-year observed crop yield data (2013–2019) for three major grain crops (wheat, maize, and rice) across China, and three major data sets including climate, vegetation indices, and soil properties were used to develop a dynamic yield forecasting system based on the random forest (RF) model. The RF model showed good performance for estimating yields of all three crops with correlation coefficient (r) higher than 0.75 and normalized root means square errors (nRMSE) lower than 18.0%. Our results also showed that crop yields can be satisfactorily forecasted at one to three months prior to harvest. The optimum lead time for yield forecasting depended on crop types. In addition, we found the major predictors influencing crop yield varied between crops. In general, solar radiation and vegetation indices (especially during jointing to milk development stages) were identified as the main predictor for winter wheat; vegetation indices (throughout the growing season) and drought (especially during emergence to tasseling stages) were the most important predictors for spring maize; soil moisture (throughout the growing season) was the dominant predictor for summer maize, late rice, and mid rice; precipitation (especially during booting to heading stages) was the main predictor for early rice. Our study provides insights into practical crop yield forecasting and the understanding of yield response to environmental conditions at a large scale across China. The methods undertaken in this research can be easily implemented in other countries with available information on climate, soil, and vegetation conditions.

Abbreviations: ML, Machine learning; RF, Random Forest; NDVI, Normalized Difference Vegetation Index; EVI, Enhanced Vegetation Index; SBD, Soil Bulk Density; SPEI, Standardized Precipitation Evapotranspiration Index; PDSI, Palmer Drought Severity Index; DEF, Climate water deficit; AET, Actual evapotranspiration; TXx, Highest daily maximum temperature; TD30, Tropical days; TNn, Coldest daily minimum temperature; FD0, Frost days; RX1day, Annual maximum 1-day precipitation; SDII, Ratio of total precipitation to wet day number.

* Correspondence authors.
E-mail addresses: yanggj@nercita.org.cn (G. Yang), yuq@nwafu.edu.cn (Q. Yu).

https://doi.org/10.1016/j.agrformet.2021.108558
Received 23 October 2020; Received in revised form 26 June 2021; Accepted 20 July 2021
Available online 27 July 2021
0168-1923/

1. Introduction

Grain crop yield forecasting is considered to be a key responsibility for food-related policy making, especially in light of soaring food demand resulting from the growing global population and increased standards of living (Tilman et al., 2011). Wheat (*Triticum aestivum* L.), maize (*Zea mays* L.), and rice (*Oryza sativa* L.) are the three major food crops around the world (Gao et al., 2019; Grundy et al., 2016), accounting for an estimated 42.5% of the world's food calorie supply (FAO, 2018). Of the three crops, wheat is the most important staple grain crop in China, and its production accounts for 18.0% of the global wheat production (Cao et al., 2020). In contrast, maize and rice production in China account for 21.4% and 30.0% of global production respectively (FAO, 2017). As a large agricultural country with more than 1.3 billion people, China must spare no effort to maintain and increase its grain crop production in order to meet the demands of a continuously increasing population in the face of shrinking arable cropland area (Yang et al., 2015).

Crop yields are significantly affected by climate and soil conditions (Alexandrov and Hoogenboom, 2000; Chakrabarti et al., 2014; Wang et al., 2016). For example, extreme high-temperature events, defined by short periods of daily maximum temperature greater than 33 °C, can greatly affect wheat and maize grain number at the early grain-filling stage (Barlow et al., 2015; Dawson and Wardlaw, 1989). Extreme cold events with daily minimum temperature less than 0 °C are closely related to crop sterility and abortion of formed grains during the flowering stage (Barlow et al., 2015). Drought and flood can also affect crop yields significantly. For instance, extreme drought affects root growth and architecture, and can result in great yield losses (Schwalbert et al., 2020); floods can directly destroy farmland, and can also cause waterlogging that is harmful to soil health and that will result in significant yield reductions (Li et al., 2019b). Soil properties have been recognized as important factors in agricultural climate change impact studies because the water and nutrient storage capacities of soils enable them to sustain crop growth in some years during periods of adverse conditions (Folberth et al., 2016; Wang et al., 2018). Thus, these soil and climatic variables can provide necessary information about the potential yields of crops, and can be used as inputs to forecast crop yields.

In addition, remote sensing data with different vegetation indices have provided good opportunities to estimate crop yields at different spatiotemporal scales due to their easy accessibility by users (Kouadio et al., 2014). Normalized Difference Vegetation Index (NDVI) and Enhanced Vegetation Index (EVI) based on MODIS (Moderate Resolution Imaging Spectroradiometer) data are two commonly-used indicators used to monitor crop growth (Kouadio et al., 2014; Son et al., 2014). In China, previous studies have used different remote sensing data to estimate crop yields (Wu et al., 2013; Zhang et al., 2020a; Zhao et al., 2013). For instance, Chen et al. (2018) used remote sensing data to derive crop phenology and leaf area index, and assimilated these two parameters into a crop model to improve the accuracy of winter wheat yield estimation at a regional scale in the North China Plain. They reported that R^2 was increased from 0.26 to 0.42 and RMSE decreased from 1012 kg/ha to 737 kg/ha. Wang et al. (2020) developed a satellite-based biophysical model (BEPS) to derive the actual rice yields and their spatial patterns in northeast China. They found that the BEPS model provided reliable estimates of rice yields in this region, with nRMSE less than 20.0% at the county level. Nevertheless, most of the previous studies only used climate data (Chen et al., 2020; Lecerf et al., 2019) or remote sensing data (Johnson et al., 2016; Mkhabela et al., 2011), and few studies have considered multi-source environmental data (e.g., climate, vegetation, and soil conditions).

Three major methods have been used to forecast crop yields: (1) field observations, (2) process-based biophysical crop simulation models, and (3) statistical models (Feng et al., 2020). Firstly, crop yield can be forecasted by crop growth information collected from field-measured data. For example, Nandram et al. (2013) forecasted maize yield based on a large farmer interview survey. However, this method is costly in terms of the time, workforce, and financial commitment required, and only provides a short time lag for decision-makers (Feng et al., 2020). Moreover, field survey methods do not fully consider all of the environmental factors affecting yield such as soil, climate, and vegetative development.

Secondly, biophysical crop models have been widely used to estimate and forecast yields (Donatelli and Confalonieri, 2011; Thorp et al., 2012; Whish et al., 2015). They can provide a deep understanding of physiological processes, and reflect the impact of interactions between crop and environmental variables (Feng et al., 2019; Zhang et al., 2020b). For example, Chen et al. (2020) used the DSSAT-CERES-Maize model to forecast maize yields and achieved an accurate estimation with absolute relative errors $<$ 8.0% when lead time was about 35 days prior to harvest. However, the effects of extreme climate-related processes are usually simplified or may not even be included in most crop models (Barlow et al., 2015; Xie et al., 2017), resulting in overestimation of the impacts of climate change on grain yield. Moreover, crop growth models usually require a substantial amount of field observation data for calibration and validation at a local scale before the models are used for long-term simulations (Burke and Lobell, 2017; Leroux et al., 2019).

Thirdly, compared with field survey methods and biophysical crop models, statistical regression-based models have the advantages of low cost and easy application, and are commonly used to estimate crop yield (Basso and Liu, 2019; Feng et al., 2018). Regression-based models include both linear regression and non-linear regression models. Some previous studies have used linear regression models to predict crop yields or have analyzed the relationship between crop yields and climate factors (Lobell and Field, 2007; Singh et al., 2010; Tao et al., 2008). However, linear regression models often had poorer performance than non-linear regression models given that crop yields have nonlinear relationships with multi-environmental factors (Feng et al., 2019; Jeong et al., 2016; Li et al., 2019c; Wei et al., 2014).

Machine learning is a new innovative approach using computational methods to "learn" information directly from data without relying on a predetermined equation as a model. It has been widely used to estimate or forecast crop yields by integrating multiple sources of environmental data (Cai et al., 2018; Puig et al., 2015). For example, Li et al. (2007) estimated corn and soybean yields using remote sensing data with multivariate regression and artificial neural network (ANN) techniques in the Midwestern and Great Plains regions of the United States. They found higher accuracy with ANN (r = 0.73–0.97 and RMSE=518–1281 kg/ha) than with multivariate regression (r = 0.58–0.93 and RMSE=868–1681 kg/ha). Cai et al. (2019) combined remote sensing and climate data with machine learning methods to estimate wheat yield in Australia, and their method had good performance (R^2=0.75). Filippi et al. (2019) used a random forest (RF) model to estimate wheat and barley grain yields using a multi-layered farm survey dataset in western Australia. Their results showed that the model could predict crop yield accurately, and had potential application in other regions where field-monitored data are available. Of the various machine learning methods, RF has been widely applied because it has high predictive capability and can provide feature importance for each variable to explain results (Everingham et al., 2016; Sonobe et al., 2014; Zhang et al., 2017). For instance, Han et al. (2020) used multi-source data in machine learning methods (Support vector machine (SVM), Gaussian process regression (GPR), and RF) to forecast winter wheat yield in China. They found RF performed best among these three machine learning methods. Maya Gopal and Bhargavi (2019) predicted paddy crop yields based on different machine learning methods (ANN, SVM, K-Nearest Neighbor, and RF) in southern India, and their results also showed that RF had better accuracy.

In China, there is an urgent need for a reliable yield forecasting system to support farmers and policy-makers. Most previous studies forecasted crop yields based on a single factor. However, even though crop yields are impacted by multiple factors, there have been few studies that have forecasted crop yields in China by using multi-source environmental factors. Recently, there have been a few studies forecasting crop yields using multi-source variables. For instance, Han et al. (2020) forecasted winter wheat yield using multi-source data and machine learning methods (SVM, GPR, and RF). Their model can successfully forecast winter wheat yield with 1–2 months lead times (R^2=0.75 and nRMSE<10.0%). Cao et al. (2020) forecasted winter wheat yield in China using multi-source data in machine learning methods, and reported a similar accuracy as observed by Han et al. (2020). Although, these wheat yield forecasting methods are very important so that stakeholders can develop early strategic decisions in their respective roles, their works were only limited to one single crop at some representative regions. However, farmers and policy-makers would prefer a crop yield forecasting system with the ability to forecast yields for many different crops over all of China. The studies reported by Han et al. (2020) and Cao et al. (2020) did not consider northwest China, an extremely important wheat production area, and thus, their methods have limited application to this region.

To bridge this gap, we developed a dynamic crop yield forecasting system based on multiple-source environmental variables for major grain crops across China (winter wheat, spring maize, summer maize, early rice, mid rice, and late rice), and investigated the key predictors determining crop yield. The results of this study will provide valuable information for policy-makers and farmers to better manage risks in order to increase agricultural production in China. The specific objectives of this study were to: (1) employ the random forest machine learning technique to create multiple models to predict yields of the three major crops using multi-source environmental data across the major grain-producing areas of China; (2) identify the optimum lead time with acceptable accuracy of yield forecast for different crops; (3) determine the most important predictors affecting crop yields.

2. Data and methods

2.1. Study area

Climate zones in China range from temperate to sub-tropical monsoon with four distinctive seasons. However, actual climate conditions vary greatly in different regions due to the large area and topographical diversification (Piao et al., 2010). For instance, annual precipitation in southern China (more than 1200 mm) is higher than in northern China (less than 600 mm), and much higher than in northwestern China (less than 200 mm) (Yao et al., 2018). This means that crops in different regions of China can be subjected to substantially different climate conditions (Tao et al., 2008). Thus, to better forecast crop yields in this study, we divided China into seven sub-regions (Fig. 1a) based on climate conditions as well as geolocation, temperature, precipitation, vegetation, and soil information (Zhao, 1983). Sub-region VI is not a main crop production area and lacks the corresponding crop yield data. Thus, we did not consider it in our analysis. See detailed information for the seven sub-regions in Yao et al. (2018) and Li et al. (2019a).

2.2. Data

2.2.1. Crop data

The crop yield trial data (including wheat, maize, and rice during 2013–2019) were collected from the National Grain Crop Growth Monitoring stations. These plot-scale experiments were conducted at each station. There were 3–5 plots (around 1 m^2 [1 m wide, 1 m long] plots for wheat and rice, and around 54 m^2 [3.6 m wide, 15 m long] plots for maize) that were randomly selected to determine one observed yield. In addition, 20 crop ears (maize) or heads (rice and wheat) were randomly selected from each plot to measure kernel number per ear and 100 (for maize) or 1000 (for rice and wheat) grain weight. Management practices were performed in keeping with local farmers' practices. These trial data were not available for all seven years at each station. Hence, there were a total of 873 samples for winter wheat, 597 for spring maize,

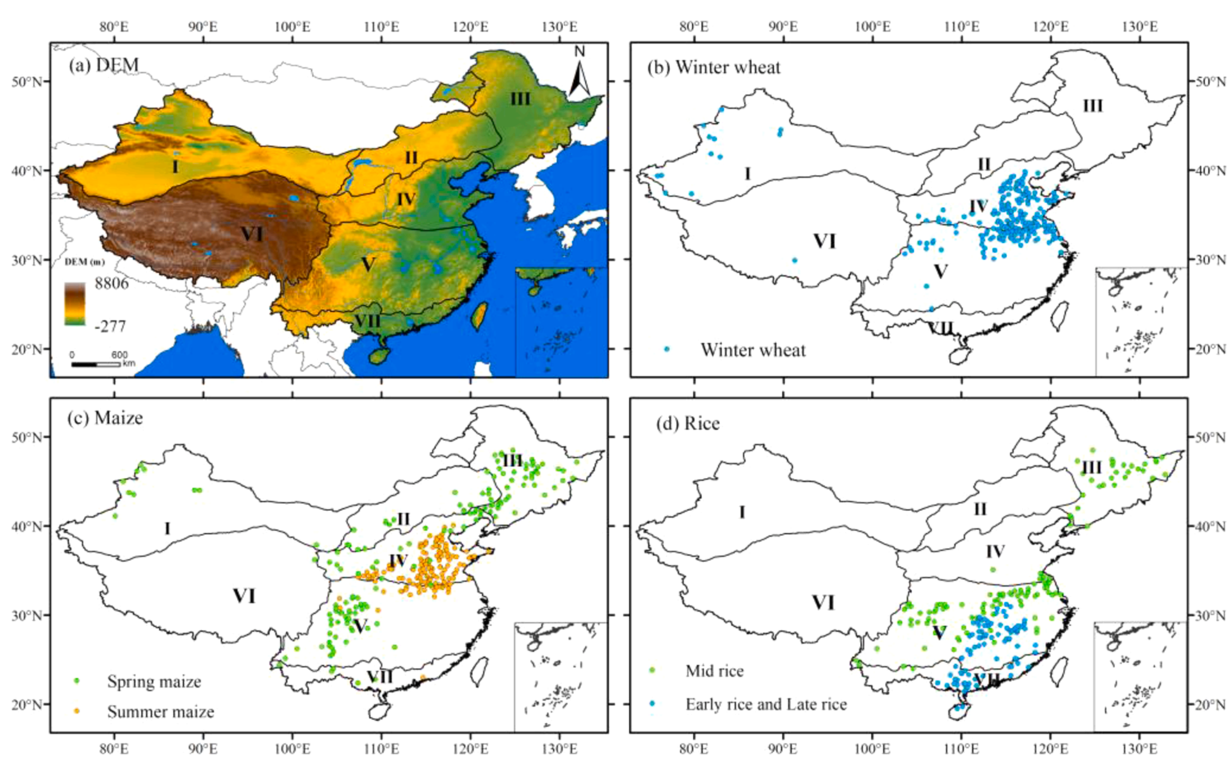

Fig. 1. Locations of seven sub-regions of China (a) and the locations of field trial sites for winter wheat (b), maize (c), and rice (d) across China.

509 for summer maize, 304 for early rice, 571 for mid rice, and 321 for late rice. These field trial data had experienced no significant technological changes in the past seven years. Thus, no de-trending approach was implemented to exclude the effects of various factors that were not reproduced by modelling. The number and spatial distribution of sites are shown in Table 1 and Fig. 1.

In this study, we considered using six main growth stages for each crop (Table 2). The growth period data were collected from the nearest agricultural meteorology stations from the China Meteorological Data Sharing Network (http://data.cma.cn/). We calculated the multi-year average of these six growth-stages as triggered successively to forecast events at each station. The days after planting during the six growth stages varied among the different crops and study regions. (Figure S1). In general, the winter wheat growing season is about 190–250 days. Winter wheat is planted from late September to early November, and harvested around early June. The maize growing season is about 100–130 days. Spring and summer maize are planted from April to May and around early June, respectively, and harvested around early September and late September, respectively. Early rice is planted in late March and harvested in July, constituting a growing season of about 100–120 days. Early rice and late rice are usually continuously cropped. Thus, the planting date of late rice is after the early rice harvest, constituting a growing season of about 110–125 days. The planting date of mid rice is about April-May, and the growing season is about 130–170 days.

2.2.2. *Climate data and extreme climate indices*

Current climate data (precipitation, temperature, and actual sunshine hours) for field trial sites from 2013 to 2019 were obtained from the nearest weather stations from the China Meteorological Data Sharing Network (http://data.cma.cn/). The sunshine hours were used to calculate the shortwave radiation (R_s) based on a relationship given in Allen et al. (1998):

$$R_S = \left[a_s + b_s\left(\frac{n}{N}\right)\right]R_a \tag{1}$$

where R_a is the extraterrestrial radiation; n and N are actual and maximum possible sunshine hours; originally a_s is 0.25 and b_s is 0.50. For better accuracy, the calibrated values of a_s and b_s at 48 stations using measured daily Rs reported by Chen et al. (2004) were used here for the nearby stations using the Thiessen polygon method (Yao et al., 2018). More information is provided in Supplementary Materials. This dataset used interpolation methods based on the WorldClim dataset, CRU Ts4.0, and the Japanese 55-year Reanalysis (Abatzoglou et al., 2018).

We selected seven extreme climate indices as predictors for forecasting crop yields (Table 3), including two extreme hot indices (i.e., TXx and TD30), three extreme cold indices (i.e., TNn, FD0, and CD10 (12)), and two extreme precipitation indices (i.e., RX1day and SDII). Five extreme climate indices (TXx, TNn, FD0, RX1day, SDII) were recommended by the Expert Team on Climate Change Detection and Indices (http://etccdi.pacificclimate.org/docs/ETCCDMIndicesComparison1.pdf). Frost days for winter wheat are defined by FD0 with minimum temperature less than 0 °C. However, the minimum temperature during the maize and rice growing seasons is greater than 0 °C in most areas. Therefore, to reflect the occurrence and impact of low-temperature conditions on maize and rice, we defined two cold temperature indices: number of cold days with minimum temperature lower than 12 °C (CD12) for maize and 10 °C (CD10) for rice (Soltani, 2012). TD30 is a user-defined index in our study because of its crucial biological implications and its suitability for each region of China. To calculate the stage-specific extreme climate indices at each site, we used the crop growth period information, including dates and duration for each crop growth stage (Table 2 and Figure S1). Therefore, each growth stage had six extreme indices (TXx, TD30, TNn, FD0 (CD10 or CD12), RX1day, SDII).

Three drought indices were also involved in this study, including Standardized Precipitation Evapotranspiration Index (SPEI), Palmer Drought Severity Index (PDSI), and Climate Water Deficit (DEF). PDSI considers the soil and evaporation, and is more suitable for revealing agricultural drought conditions. SPEI is based on the water balance, and can monitor drought conditions associated with water demand (Vicente-Serrano et al., 2010). Monthly SPEI was used as an explanatory predictor. DEF can effectively integrate the combined effects of solar radiation, evapotranspiration, and air temperature on watershed conditions given available soil moisture derived from precipitation (Stephenson, 1998).

We extracted monthly AET, DEF, and PDSI data for each study site based on the Google Earth Engine (GEE) platform and calculated the monthly site-scale SPEI based on its definition (Table 3), then selected the value in the month that was closest to each crop growth stage. For other site-scale climate indices, we derived their values based on the definitions in Table 3 at each growth stage for each site.

2.2.3. *Vegetation data*

Vegetation indices (e.g., NDVI and EVI) can reflect the crop growth condition (Han et al., 2020; Kouadio et al., 2014; Wu et al., 2013). Therefore, in this study, NDVI and EVI were used as additional predictors in crop yield forecasting. Moreover, these indices have wide coverage and high resolution, and can easily be applied in other regions (Son et al., 2014). Here, the NDVI and EVI (2013–2019) data were downloaded from the MOD13A1 V6 (https://lpdaac.usgs.gov/products/mod13a1v006/), with 16-day repeat and 500 m spatial resolution. We extracted NDVI and EVI values for each study site based on the GEE platform. Then we calculated the average of NDVI and EVI for each crop growth stage at each site.

2.2.4. *Soil data*

The soil moisture data were downloaded from the Global Land Data Assimilation System (GLDAS). Using advanced land surface modeling and data assimilation techniques, GLDAS generates optimal fields of land surface states and fluxes (https://ldas.gsfc.nasa.gov/gldas/) by the GEE platform. The soil moisture data at 0–10 cm, 10–40 cm, 40–100 cm, and 100–200 cm were used in this study. The soil moisture data have been evaluated by comparison with measured values, and were found to

Table 1
The number of field trial sites for six types of crops in six different sub-regions of China identified in Fig. 1.

Crop types	Sub-region I	II	III	IV	V	VII
Winter wheat	12	\	\	131	77	\
Spring maize	10	16	50	26	48	5
Summer maize	\	\	\	123	27	\
Early rice	\	\	\	\	61	32
Mid rice	\	\	29	8	90	4
Late rice	\	\	\	\	61	32

Table 2
Six growth-stages used for wheat, maize, and rice. The days after planting (DAP) for different growth stages in different regions are shown in Figure S1.

Time interval	Crop Winter wheat	Maize (spring and summer maize)	Rice (early, mid, and late rice)
T1	planting-emergence	planting-emergence	planting-emergence
T2	emergence-tillering	emergence-three leaves	emergence-tillering
T3	tillering-jointing	three leaves-six leaves	tillering-booting
T4	jointing-heading	six leaves-tasseling	booting-heading
T5	heading-milk	tasseling-milk	heading-milk
T6	milk-maturity	milk-maturity	milk-maturity

Table 3
Environmental variables used in crop yield forecast during 2013–2019 in China.

Type		Term	Definition	Resolution Temporal	Resolution Spatial	Data source
Climate	Weather data	Pr (mm)	Total precipitation	daily	site	http://data.cma.cn/ Same as above Same as above
		Tmean (°C)	Mean temperature	daily	site	
		Rad (MJ/m^2)	Mean shortwave radiation*	daily	site	
		AET (mm)	Actual evapotranspiration	monthly	0.1° × 0.1°	http://www.climatologylab.org/terraclimate.html Same as above Same as above
	Drought Indices	PDSI	Palmer Drought Severity Index	monthly	0.1° × 0.1°	
		DEF (mm)	Climate water deficit	monthly	0.1° × 0.1°	
		SPEI	Standardize Precipitation Evapotranspiration Index	monthly	site	Calculated by Vicente-Serrano et al. (2010)
	Extreme temperature	CD10(12) (Day)	Number of days with daily Tmin <10 (12) °C	Growth stage	Site	User defined
		TD30 (Day)	Number of days with daily T_{max} >30 °C	Growth stage	Site	User defined
		FD0 (Day)	Number of days with daily T_{min} <0 °C	Growth stage	site	Defined by Expert Team on Climate Change Detection and Indices (http://etccdi.acifificclimate.org/docs/ETCCDMIndicesComparison1.pdf)
		TNn (°C)	Lowest daily T_{min}	Growth stage	site	
		TXx (°C)	Highest daily T_{max}	Growth stage	Site	
	Extreme precipitation	RX1day (mm)	Annual maximum 1-day Pr	Growth stage	Site	Same as above
		SDII (mm/day)	The ratio of total Pr to wet day number (≥ 1 mm)	Growth stage	Site	Same as above
Vegetation		NDVI	Normalized Difference Vegetation Index	16-day	500 m	https://lpdaac.usgs.gov/products/mod13a1v006/
		EVI	Enhance Vegetation Index	16-day	500 m	Same as above
Soil		Soil moisture (kg/m^3)	Soil moisture	3-hour	0.25° × 0.25°	https://ldas.gsfc.nasa.gov/gldas/

* Sunshine hours were used to calculate the shortwave radiation based on a relationship given in Allen et al. (1998).

be accurate across China (Liu and Zhao, 2018; Liu et al., 2019). The areal resolution of this dataset was 0.25° × 0.25°, and the temporal resolution was three hours. In this study, we calculate the average of soil moisture over each crop growth stage at each site. The unit of soil moisture data is kg/m^2. In order to unify the unit, the soil moisture values at different depths were converted to m^3 m^{-3} (%) by the following equation:

$$\theta = \frac{\omega}{\rho \times h} \times 100\% \tag{2}$$

where, θ is the volumetric soil water content (%); w is the GLDAS soil moisture (kg/m^2); ρ is the density of water (kg/m^3), ρ = 1000 kg/m^3; h is the soil layer thickness (m).

2.3. Modeling methodology

2.3.1. Random forest and modeling framework

The RF model is an ensemble learning method for regression based on constructing a multitude of decision trees (Breiman, 2001). The regression tree was constructed independently, and was based on independent samples of the original dataset. The RF model can roughly estimate both linear and nonlinear relationships. Moreover, RF can also provide reliable information about the feature importance of each variable and effectively estimate test error with low computational cost of the training model (Stefan, 2018). We assessed the relative importance through the "%IncMSE" from the RF model. The%IncMSE indicates the mean decrease of accuracy (test by mean square error) in nodes that use a variable in the RF model when values of the variable are randomly permuted (Feng et al., 2018). Some previous studies have shown that the performance of the RF model is usually better than many other machine learning methods in the field of agricultural studies (Feng et al., 2019; Wang et al., 2018).

We optimized the two RF model hyperparameters: number of variables randomly sampled as candidates at each split (m_{try}) and number of trees to grow (n_{tree}). The range of m_{try} was defined from 1 to the number of variables with 1 interval, and the range of n_{tree} was set from 200 to 1200 with 200 intervals. In this study, we selected the optimum hyperparameters with the smallest error for each RF model (Table S1). The optimal m_{try} and n_{tree} were chosen by the 'tuneRF' function that uses Out-Of-Bag (OOB) data to perform unbiased internal validation. Since random forest uses bootstrap to construct each "tree", one-third of data normally are not involved in construction of "trees", and these data are called OOB data (Breiman, 2001). The 'tuneRF' function calculates OOB error based on different mtry, and relatively lower OOB errors indicate better model performance (Breiman, 2001). In this study, we used 'tuneRF' by setting different n_{tree} in order to optimize m_{try}. The RF model and 'tuneRF' function were implemented by R (version 3.6.0) software (www.r-project.org) using the 'randomForest' package (https://cran.r-project.org/web/packages/randomForest/index.html). The data analysis code in this study is available (https://github.com/llinchao/yield_forecast).

We developed a yield forecasting system based on multi-source environmental data using the RF algorithm. We first aggregated the multi-source environmental variables into six groups by different growth stages (from T1 to T6) for each crop type. The forecasting events were then triggered successively at each growth stage, and the predictors were added with crop growth progression. The forecasting events were then triggered successively at each growth stage, and the predictors in each phase were added with crop growth progression. Therefore, the number of predictors increased with progressing phases from T1 to T6. To demonstrate the most important predictors at different stages, the relative importance of each covariate was calculated by averaging them throughout phases. For instance, the relative importance of NDVI at T3 is averaged by NDVI at T1 (NDVI_1), NDVI at T2 (NDVI_2), and NDVI at T3 (NDVI_3). In this study, the stage-specific variables (e.g., extreme climate indices, vegetation indices, and soil moisture) were considered (refer to Table 3), and therefore, our yield forecasting system could dynamically forecast the crop yields at the end of several targeted growth stages (T1-T6) as the growing season progressed to maturity. In our yield forecasting system, we developed an individual RF model for each crop type. In addition, the forecasting events based on T1-T6 (Table 2) varied for different crops (Figure S1). The overall modeling framework is shown in Fig. 2 and demonstrates how we developed each individual RF model based on multiple predictors at different growth stages (T1-T6, see Table 2).

2.3.2. Model performance assessment

The leave-one-year-out cross validation method (Molinaro et al., 2005) was used to evaluate the model performance for the six crops (winter wheat, spring maize, summer maize, early rice, mid rice, and late rice). In this study, we used Pearson's correlation coefficient (r) and normalized root mean square error (nRMSE) to assess model performance. The equations are written as follows:

$$r = \frac{\sum_{i=1}^{n}(x(i)-\overline{x})(y(i)-\overline{y})}{\sqrt{\sum_{i=1}^{n}(x(i)-\overline{x})^2}\sqrt{\sum_{i=1}^{n}(y(i)-\overline{y})^2}} \tag{3}$$

$$RMSE = \sqrt{\frac{\sum_{i=1}^{n}(x(i)-y(i))^2}{n}} \tag{4}$$

$$nRMSE = \frac{RMSE}{\overline{x}} \tag{5}$$

where y(*i*) and *x*(*i*) are the *i*th forecasted and observed yield values, respectively; $\overline{y}$ and $\overline{x}$ represents the mean of forecasted and observed values; *n* is the number of samples.

In this study, we used the 'ggplot2' R package to make figures (Wickham, 2011). Spatial distributions of field trial sites were mapped using the ArcGIS 10.3 software.

3. Results

3.1. Accuracy of yield forecasts

The wheat, maize, and rice yields varied in each sub-region (Fig. 3). Observed values of, winter wheat yield ranged from 1952 to 8804 kg/ha, spring maize ranged from 2997 to 17,370 kg/ha, summer maize ranged from 4127 to 10,889 kg/ha, early rice ranged from 4607 to 8853 kg/ha, mid-season rice ranged from 5291 to 12,185 kg/ha, and late rice ranged from 4811 to 9436 kg/ha. The median winter wheat yield in the North China Plain (sub-region IV) was higher than in sub-regions I and V. The median spring maize yields followed the order of sub-region VII<V<IV<II<III<I. The median summer maize yield in sub-region IV was higher than in sub-region V. The median yields of early rice were similar in sub-regions V and VII, and late rice yields in sub-region V were

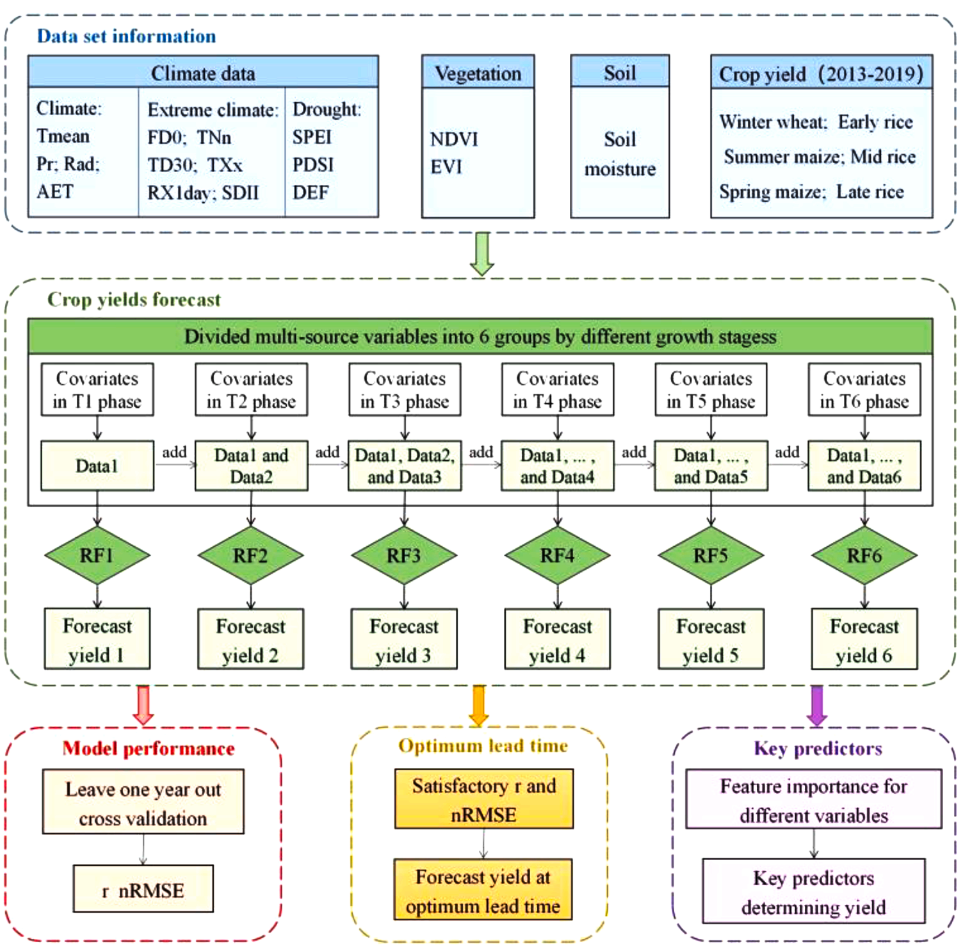

Fig. 2. Schematic overview of data input and output for the RF model developed in this study. T1 to T6 represent the six growth stages for each crop type (Table 2).

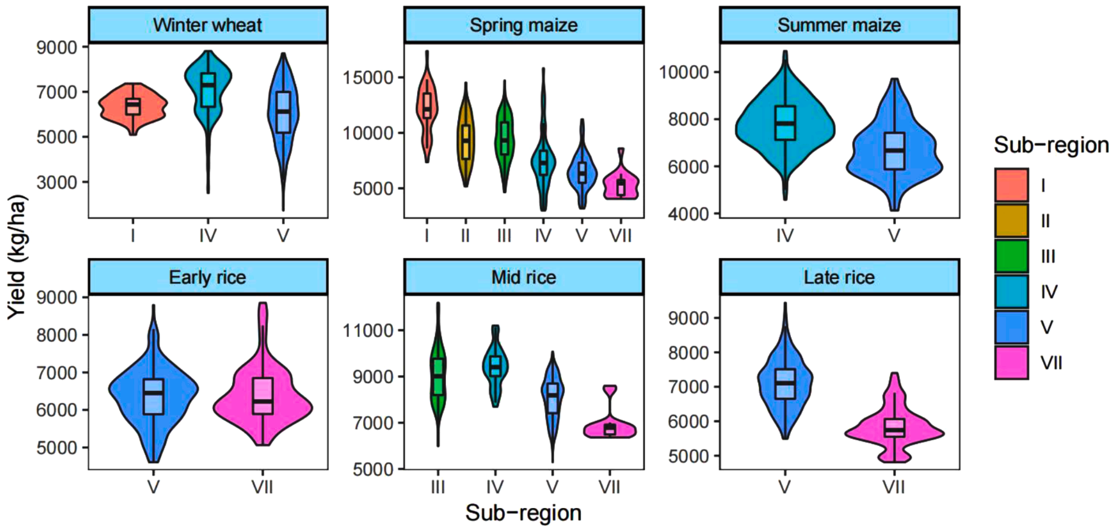

Fig. 3. Distribution of measured crop yields in six different sub-regions of China during 2013–2019. Box boundaries in the violin plot indicate the 25th and 75th percentiles of crop yields, whiskers below and above the box indicate the 10th and 90th percentiles. The black lines within each box indicate the median value. The violin plot outlines illustrate kernel probability density, i.e., the width of the shaded area represents the proportion of the crop yield data located there. (For interpretation of the references to colour in this figure legend, the reader is referred to the web version of this article.)

higher than in sub-region VII. The median mid rice yields followed the order of sub-region VII<V<III<IV (Fig. 3). The reasons for the yield variability are likely attributable to differences in soil, weather conditions, drought, extreme climate events, etc. Therefore, forecasting crop yields based on multi-source environmental variables will be a valuable contribution.

To better understand the stability of model performance, we showed r and nRMSE values at different lead times for the six crop types across all (left out) years (Fig. 4 and Table S2). Model performance, as stated above, was evaluated by r and nRMSE. Fig. 4 shows the cross-validation accuracy metrics for the forecasted yield of six crops based on the RF model across all (left out) years including 2013–2019. The performance of the model generally improved as the predictive period approached the end of the growing season (i.e., r gradually increased and nRMSE decreased with time). The forecast of winter wheat yield was relatively poor at T1 ($r = 0.65$ and nRMSE=14.6%), and forecast accuracy greatly increased at and after T3 (tillering-jointing). The value of r increased from 0.65 (T1) to 0.81 (T3) and nRMSE decreased from 14.6% (T1) to 11.4% (T3). The forecast of spring maize yield was relatively accurate because the r values went from 0.71 (T1) to 0.84 (T6), but the nRMSE values were relatively high (16.2–20.4%). The performance of summer maize yield forecast greatly increased from T1 (0.68) to T4 (0.77) and nRMSE decreased from 11.3% (T1) to 10.4% (T4). The accuracy of yield forecasts for early rice increased significantly at T4. The r of forecasted mid rice yield increased from 0.68 (T1) to 0.84 (T6), and the nRMSE decreased from 9.6% (T1) to 7.2% (T6). The r of forecasted late rice yield increased greatly from 0.68 (T1) to 0.79 (T6), and the nRMSE decreased from 9.8% (T1) to 8.4% (T6). In general, the RF model had satisfactory performance, and most crops had r higher than 0.75 and nRMSE lower than 18.0% before the end of the growing season. Thus,

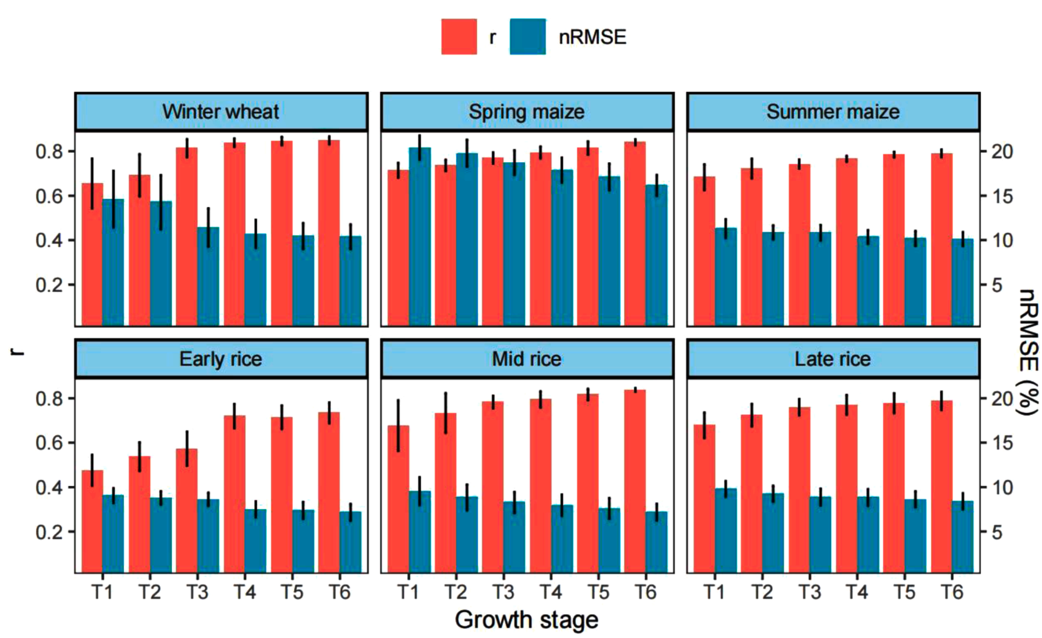

Fig. 4. Model performance at different forecasting times (growth stages) for six crop types based on the evaluation for each (left out) year during 2013–2019. The filled bars represent the mean values of r and nRMSE; the error bars represent the standard errors for seven years.

results show that the RF model using multi-source data can forecast crop yields accurately, and indicate that this yield forecasting approach can provide reliable yield projections. Also, the stability of our yield forecasting system increased as accuracy increased from T1 to T6 for each crop.

The model's performance in different sub-regions for each crop is shown in Figures S2-S4. Model performance was evaluated across all (left out) years at once for each sub-region due to the limited number of sampling points in some years. Our results showed that model performance was varied in different sub-regions even for the same crop. This was mainly due to differences in the number of sampling points used in each subregion (Table 1). For instance, the *r* values of the summer-maize model in sub-region V (r = 0.73–0.78 during T1-T3) were higher than sub-region IV (r = 0.58–0.65 during T1-T3), while the nRMSE values were similar. Nonetheless, the *r* of the summer maize model in sub-region IV showed a great increase during T4-T6 and reached similar results between sub-region IV and V at T6. Generally, the predictive capacity of each RF model showed a gradual increase as the growing season progressed towards maturity in most sub-regions.

3.2. The optimum lead time provided by yield forecasts

Based on the accuracy of the yield forecasts for the six crops at different growth stages, the optimum lead time provided by the yield forecasting system could be identified. In general, forecast accuracy increased with crop growth and development, and the rate of increase slowed down at later growth stages. In order to reveal the magnitude of changes observed for each model performance during T1 to T6, we normalized the r and nRMSE from 0% to 100% (expressed as r_n and $nRMSE_n$), as illustrated in Fig. 5 (see method details in Feng et al. (2020)). For instance, the greatest increase in model performance occurred during T2 to T3 for winter wheat, in which r_n increased by 62.7% and $nRMSE_n$ decreased by 67.5% (Fig. 5). However, model accuracy increased slightly after T4. Therefore, T4 can be selected as an appropriate lead time in yield forecasts. As another example, the forecast accuracy for early rice increased greatly at T4 (booting to heading, r_n increased by 56.7% and $nRMSE_n$ decreased by 60.5%), while after T4, there was only a slight improvement (r_n increased by 5.7% and $nRMSE_n$ decreased by 17.7%). Generally, most crops could reach a satisfactory model performance.

In general, crop yields can be satisfactorily forecasted with the RF model (Table S3, Fig. 5) at around one to three months prior to harvest for winter wheat (r = 0.81–0.85, nRMSE=10.5–11.4%); one to two months before harvest for spring maize (r = 0.79–0.81, nRMSE=17.1–17.9%), summer maize (r = 0.77–0.79, nRMSE=10.2–10.4%), early rice (r = 0.71–0.72, nRMSE=7.4–7.5%), mid rice (r = 0.78–0.82, nRMSE=7.6–8.3%), and late rice (r = 0.76–0.78, nRMSE=8.6–8.9%).

3.3. Predictor importance

The feature importance of each predictor variable was used to reflect the contribution of different predictors to forecast yield (Fig. 6). In general, Pr, Soil, and VIs were identified to be major predictors for yield forecasting. However, the major predictors varied for different crops. For instance, soil moisture was the major predictor for winter wheat yield forecasts during T1-T2. After T3, solar radiation (Rad) and VI were the main predictors for winter wheat yield forecasts. The main yield predictors for spring maize were vegetation indices (NDVI and EVI) and drought indices (DI) especially during T2-T5. Soil moisture and VI were the main predictors for summer maize yield throughout the growing season. Pr (throughout the growing season, especially at T4) and ETH (at T6) were the most important predictors for early rice yield forecasts. Soil moisture was the main predictor for mid rice and late rice throughout the growing season. In addition, extreme cold event (ETC) was also identified as important yield predictor for late rice during T1-T2. In this study, we found the importance of NDVI and EVI in forecasting yield were not highly ranked for rice (early rice, mid rice, and late rice).

4. Discussion

4.1. Model performance

Many studies have estimated wheat, maize, and rice yields by crop models (Li et al., 2014; Palosuo et al., 2011), statistical methods (Fan et al., 2020; Jiang et al., 2020), and hybrid approaches using a bio-physical model and machine learning techniques (Feng et al., 2019). Silvestro et al. (2017) estimated winter wheat yield using remote sensing data (LAI and canopy cover) with two crop models (AquaCrop and a simple algorithm with the ensemble Kalman filter) at Yangling located in northwest China, and the lowest nRMSE (18.0%) was found using their simple algorithm model. Comparing their results with our work, we had a higher accuracy (nRMSE=10.4%) of yield estimation. Liu et al. (2017a) estimated maize yields in the North China Plain using the

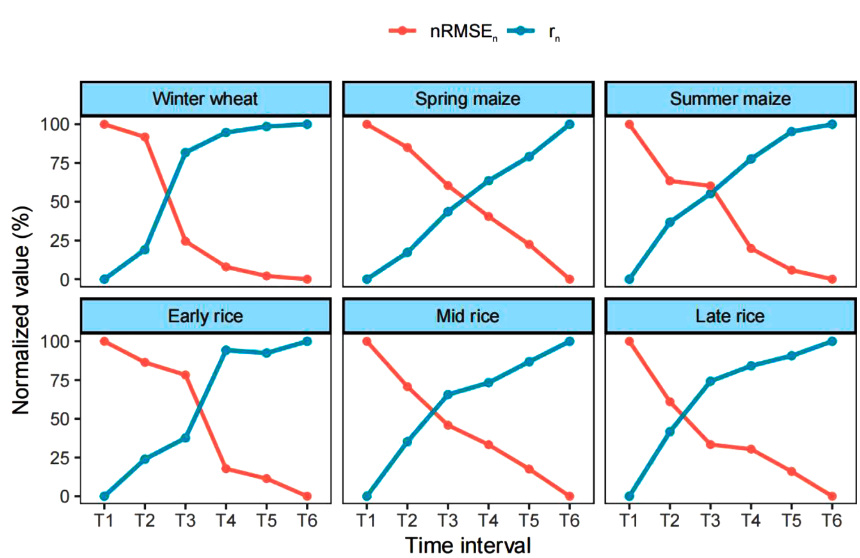

Fig. 5. Normalized values of the model performance measures (r_n and $nRMSE_n$) at six time-intervals (growth stages) for winter wheat, spring maize, summer maize, early rice, mid rice, and late rice using the RF-based forecasting model to predict crop yield in China (2013–2019). (For interpretation of the references to colour in this figure legend, the reader is referred to the web version of this article.)

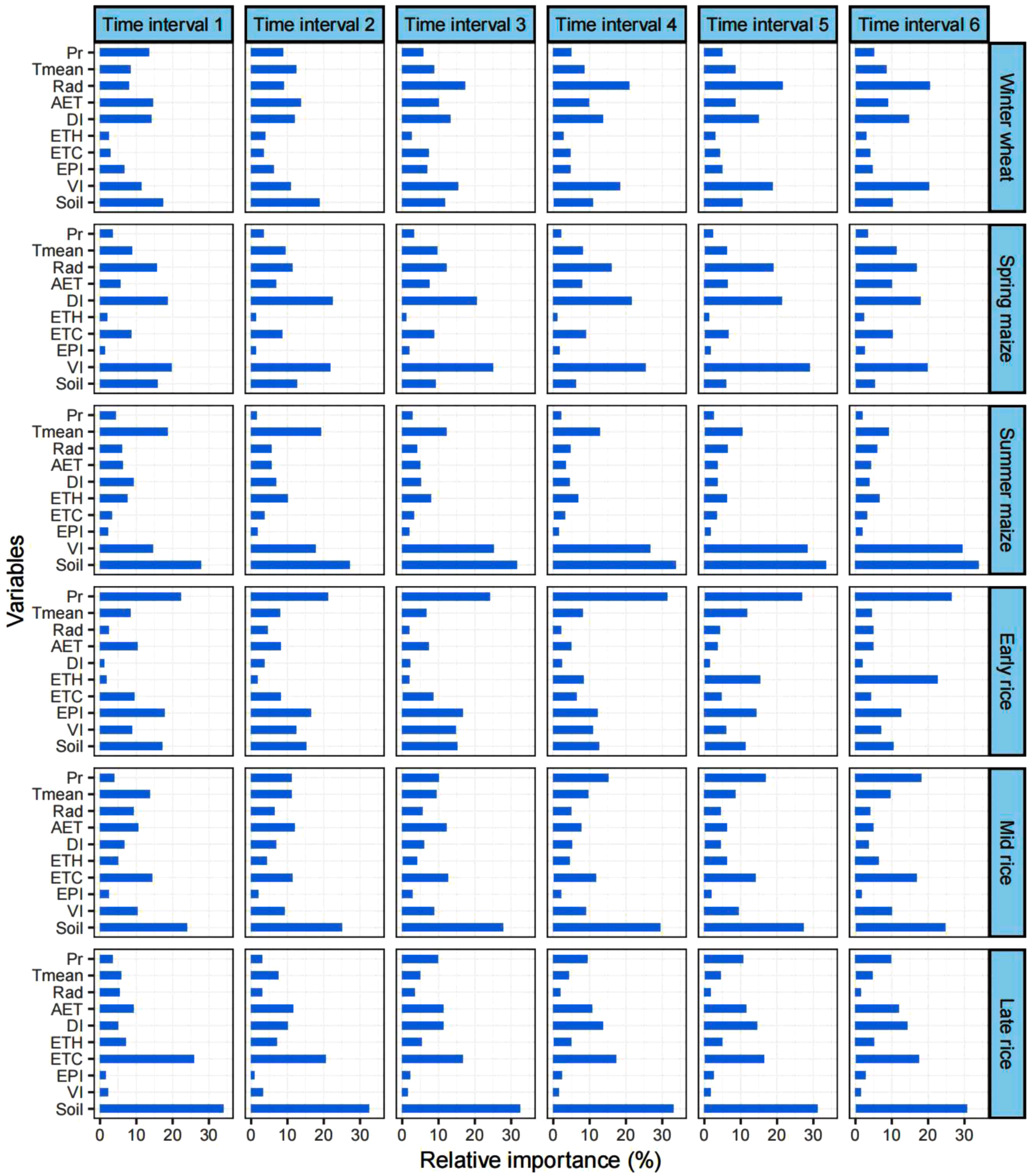

Fig. 6. The relative importance of predictor variables at different time intervals for six crop types. The importance of each variable was based on the percentage increase of mean square error from the RF model. We normalized relative importance values so that they summed to 100%. (AET: actual evapotranspiration; EPI: extreme precipitation indices (RX1day and SDII); ETC: extreme cold temperature indices (cold days (FD0, CD10, or CD12) and TNn); ETH: extreme hot temperature indices (TD30 and TXx); Rad: shortwave radiation; Soil: soil moisture; Pr: precipitation; VI: vegetation indices (NDVI and EVI); DI: drought indices (SPEI, PDSI and DEF); Tmean: mean temperature). (For interpretation of the references to colour in this figure legend, the reader is referred to the web version of this article.)

DSSAT model (r = 0.67–0.85 and nRMSE=26.8–29.8%). These values were similar to our r values (0.84 for spring maize and 0.79 for summer maize), but we found lower nRMSE (16.2% for spring maize and 10.1% for summer maize) with our work. Guo et al. (2020) predicted rice yields using phenology and climate data in machine learning models in China, and reported r values of 0.49–0.57, while our study had better performance (r = 0.73, 0.84, and 0.79 for early rice, mid rice, and late rice, respectively). Son et al. (2014) incorporated NDVI, EVI, and rice yield statistics into a quadratic regression model to estimate rice yields in South Vietnam during the spring–winter (r = 0.79–0.84 and nRMSE=6.9–8.1%) and summer–autumn (r = 0.63–0.75 and nRMSE=5.4–6.7%), and these values were similar to our results (r = 0.73–0.84 and nRMSE=7.2–8.4%). In summary, our study was able to achieve similar or even better performance in yield prediction for different crop types than most previous studies.

In addition, our work found that model performance varied for different sub-regions and crop types. This finding was mainly because our yield forecasting system was data-driven, and therefore, the crop type data, data volume, and data quality were key factors in determining model accuracy (Peng et al., 2020). In our study, the number of trial data sets, variability of crop yields, climate conditions, and the size of the study area were variable in each sub-region (Table 1 and Fig. 3). These variations can impact model performance regionally. In addition, model performance also varied with years. It is interesting to note that model performance for early rice in T1-T3 was low in 2013–2019 (Table S2). This result was largely due to the relatively small number of trial data sets for early rice (304 sets of trial data) compared with other crop types (Fig. 1 and Table 1).

4.2. Wheat yield forecasts

In this study, we forecast winter wheat yield with satisfactory accuracy (r = 0.81–0.85, nRMSE=10.5–11.4%) at one to three months lead time. This result was consistent with a previous study of Cao et al. (2020) that forecast winter wheat yields over the North China Plain during 2001–2015 based on multi-source environmental parameters and three machine learning approaches. In our study, the important predictor for winter wheat yield during T1-T2 (planting-tillering) stages was soil moisture (Fig. 6). This may be because drought stress impacts the potential tillering capacity of wheat. Moreover, a dry soil condition often affects the development of the coleoptile and first tillers, and thus influences the tiller number per plant (Blum et al., 1990). Forecast accuracy was greatly increased at T3, probably because of stabilized wheat growth after tillering (e.g., fertilization) (Otteson et al., 2008). Moreover, during the tillering stage, wheat had already produced the important yield trait of number of tillers. Therefore, during these stages, the farmer should give greater attention to irrigation and nitrogen management, both of which can greatly impact tiller number (Blum et al., 1990; Otteson et al., 2008). In addition, number of wheat tillers can also be improved by selecting the optimum seeding rate based on an appropriate target plant density (Bastos et al., 2020). After the T3, radiation and vegetation indices were determined to be the main predictors determining wheat yield. Solar radiation is one of the primary limiting factors in wheat yield after T3 because winter wheat biomass is produced by photosynthesis in green plant tissues, especially during T4-T5 (jointing to milk development stages) (Li et al., 2008; Mu et al., 2010), and photosynthesis rate is mainly influenced by solar radiation.

4.3. Maize yield forecasts

The optimum lead time was around one to two months for spring maize (r = 0.79–0.81, nRMSE=17.1–17.9%) and summer maize (r = 0.77–0.79, nRMSE=10.2–10.4%). Meng et al. (2014) forecast maize yields in northeastern China based on remote sensing data and regression methods, and their results showed that the lead time was 55–60 days after the stage of seeding establishment, and the accuracy (nRMSE=7.3–16.9%) was similar to our results. However, they did not consider additional environmental variables (e.g., drought and extreme climate events), and their work was limited to county-level rather than field level. In this study, drought indices were identified as the main predictors, most especially around the tasseling stage, meaning that drought during this time interval was the main influence on spring maize yield. Many previous studies have also found that the spring maize tasseling stage is a highly drought-sensitive period (Atteya, 2003; Gao et al., 2017). Supplemental irrigation at the tasseling stage can increase the post-silking water consumption percentage that results in more water and soil nitrogen allocated for grain growth and development, ultimately reducing the risk of yield losses (Gao et al., 2017). In addition, our results also showed that the forecast accuracy for summer maize was greatly increased at T4 (six leaves-tasseling), and increased slightly during T5-T6. The explanation for this result is that after the tasseling stage (T4) the canopy is fully developed with maximum capacity for radiation interception (Chen et al., 2020), and therefore, the forecast of the final yield is more certain.

4.4. Rice yield forecasts

Notably, no such forecast model as we have reported here has been established for rice across China. We expect within-season yield forecasting for rice can fill the knowledge gap for the rice industry in China. Generally, rice yield can be forecasted with a satisfactory accuracy at different lead times (Fig. 4 and Table S3). Soil moisture was one of the main factors causing instability in crop yield (Rossato et al., 2017; Singh et al., 2017). In this study, soil moisture was identified as the most important predictor for determining mid rice and late rice yield throughout the entire growing season. This was because soil water conditions not only influence pollen and embryo development (Royo et al., 2006), but also affect the translocation of photosynthate for aboveground growth and underground growth, especially during the grain filling stage (Chaves et al., 2002). In addition, low temperature was also identified as one of the main influence factors for late rice yield forecasts. This is because low temperatures may influence the number of tillers (during T1-T2), cause pollen abortion (during T3-T4), and retard rice growth (Moldenhauer and Slaton, 2001). Our work also showed that yield forecast accuracy was increased greatly for early rice at T4 (Fig. 5). This result was probably because T4 (booting-heading) is sensitive to climate conditions, and has been identified in previous studies as the key stage in determining rice yield formation, which has been reported in previous studies (Asch et al., 1999; Chang et al., 2005; Fageria, 2007). Therefore, producers should optimize the nutrient management practices especially at these stages. For instance, Sui et al. (2013) found that high N application at the early vegetative stage can increase the number of panicles. In addition, adjusting the proportion of N application at different growth stages can improve the source-sink conflict associated with yield development, and consequently increase rice yield. In this study, vegetation indices were the main predictors for wheat and maize yield, but were found to be not highly important for rice yield prediction. This result may be due to the unclosed rice canopy and soil background features, both of which impact the canopy spectral sensor, thus further influencing these vegetation indices used in estimating rice yield (Liu et al., 2017b).

Generally, our within-season yield forecasting system can support these stakeholders to monitor the dynamics of crop yields and provide a scientific basis for establishment of policy and risk management. Nevertheless, there is a trade-off between model performance and lead time in the yield forecasting system (Feng et al., 2020). Therefore, stakeholders could select the optimal forecast lead time based on different purposes.

4.5. Limitations and future framework

We developed a yield forecasting system in this study to predict crop yields for three major crops in China. However, there are some limitations in this modelling work. Firstly, we did not consider and account for field management options (e.g., irrigation and fertilization) due to insufficient observed data, and this may have effects on the accuracy of yield forecasts. Secondly, cultivar selection is also an important management factor determining crop yields (Xiao et al., 2020). Different genotypes will have significant impacts on yield in different growing regions. However, we did not include different cultivar types in our model due to lack of data. Thirdly, we did not use the observed phenological data to accurately incorporate crop growth stage into the model. Feng et al. (2020) acquired crop phenology information by dynamically running biophysical model simulations and developed machine learning models by using stage-specific predictors. Therefore, developing a hybrid approach using a biophysical model and machine learning technique might be a good choice in the future to improve the accuracy of crop yield forecasts (Feng et al., 2019; Shahhosseini et al., 2021).

5. Conclusions

We developed yield forecasting systems for three major crops with a machine learning method using multi-source environmental variables and different field trial sites across China. Our study showed that using machine learning driven by multi-source environmental variables can provide satisfactory crop yield forecasts. Overall, our model performance for each crop was comparable with results from previous studies. We found that yield could be satisfactorily forecast at around one to three months prior to harvest for winter wheat (r = 0.81–0.85, nRMSE=10.5–11.4%); one to two months before harvest for spring maize (r = 0.79–0.81, nRMSE=17.1–17.9%), summer maize (r = 0.77–0.79, nRMSE=10.2–10.4%), early rice (r = 0.71–0.72, nRMSE=7.4–7.5%), mid rice (r = 0.78–0.82, nRMSE=7.6–8.3%), and late rice (r = 0.76–0.78, nRMSE=8.6–8.9%). We expect that the different lead times identified by our machine learning forecast model can provide valuable information for farmers and policy-makers to reduce the risk of yield loss before the end of the growing season. We also identified the main predictors that determine wheat, maize, and rice yields. Generally, solar radiation and vegetation indices (especially during jointing to milk development stages) were identified as the main predictor for winter wheat; vegetation indices (throughout the growing season) and drought (especially during emergence to tasseling stages) were the most important predictors for spring maize; soil moisture (throughout the growing season) was the dominant predictor for summer maize, late rice, and mid rice; precipitation (especially during booting to heading stages) was the main predictor for early rice. Our future work will develop a hybrid approach using a biophysical model and a machine learning technique to improve the accuracy of crop yield forecasts.

Declaration of Competing Interest

The authors declare that they have no known competing financial interests or personal relationships that could have appeared to influence the work reported in this paper.

Acknowledgments

This study was supported by the Natural Science Foundation of China (no. 41961124006), National Key Research and Development Program of China (2019YFE0125300, 2017YFE0122500), Natural Science Foundation of Qinghai (2021-HZ-811), and Key-Area Research and Development Program of Guangdong Province (2019B020216001).

Supplementary materials

Supplementary material associated with this article can be found, in the online version, at doi:10.1016/j.agrformet.2021.108558.

References

Abatzoglou, J.T., Dobrowski, S.Z., Parks, S.A., Hegewisch, K.C., 2018. TerraClimate, a high-resolution global dataset of monthly climate and climatic water balance from 1958 to 2015. Sci. Data 5, 170191.
Alexandrov, V.A., Hoogenboom, G., 2000. The impact of climate variability and change on crop yield in Bulgaria. Agric. For. Meteorol. 104 (4), 315–327.
Allen, R.G., Pereira, L.S., Raes, D., Smith, M., 1998. Crop evapotranspiration-guidelines for computing crop water requirements. FAO Irrigation and Drainage Paper 56. FAO, Roma, Italia.
Asch, F., Dingkuhn, M., Wittstock, C., Doerffling, K., 1999. Sodium and potassium uptake of rice panicles as affected by salinity and season in relation to yield and yield components. Plant Soil 207 (2), 133–145.
Atteya, A., 2003. Alteration of water relations and yield of corn genotypes in response to drought stress. Bulg. J. Plant Physiol 29 (1–2), 63–76.
Barlow, K.M., Christy, B.P., O'Leary, G.J., Riffkin, P.A., Nuttall, J.G., 2015. Simulating the impact of extreme heat and frost events on wheat crop production: a review. Field Crop. Res. 171, 109–119.
Basso, B., Liu, L., 2019. Seasonal crop yield forecast: methods, applications, and accuracies. Adv. Agron. 201–255.
Bastos, L.M., et al., 2020. Winter wheat yield response to plant density as a function of yield environment and tillering potential: a review and field studies. Front. Plant. Sci. 11, 54.
Blum, A., Ramaiah, S., Kanemasu, E., Paulsen, G., 1990. Wheat recovery from drought stress at the tillering stage of development. Field Crop. Res. 24 (1–2), 67–85.
Breiman, L., 2001. Random forests. Mach. Learn. 45 (1), 5–32.
Burke, M., Lobell, D.B., 2017. Satellite-based assessment of yield variation and its determinants in smallholder African systems. Proceed. Natl. Acad. Sci. 114 (9), 2189–2194.
Cai, Y., et al., 2019. Integrating satellite and climate data to predict wheat yield in Australia using machine learning approaches. Agric. For. Meteorol. 274, 144–159.
Cai, Y., et al., 2018. A high-performance and in-season classification system of field-level crop types using time-series Landsat data and a machine learning approach. Remote Sens. Environ. 210, 35–47.
Cao, J., et al., 2020. Identifying the contributions of multi-source data for winter wheat yield prediction in China. Remote Sens. (Basel) 12 (5).
Chakrabarti, S., Bongiovanni, T., Judge, J., Zotarelli, L., Bayer, C., 2014. Assimilation of SMOS soil moisture for quantifying drought impacts on crop yield in agricultural regions. IEEE J. Sel. Top. Appl. Earth Obs. Remote Sens. 7 (9), 3867–3879.
Chang, K.-.W., Shen, Y., Lo, J.-.C., 2005. Predicting rice yield using canopy reflectance measured at booting stage. Agron. J. 97 (3), 872–878.
Chaves, M.M., et al., 2002. How plants cope with water stress in the field. Photosynthesis and growth. Ann. Bot. 89, 907–916. Spec No:
Chen, R., Ersi, K., Yang, J., Lu, S., Zhao, W., 2004. Validation of five global radiation models with measured daily data in China. Energy Conver. Manag. 45 (11–12), 1759–1769.
Chen, S., et al., 2020. Dynamic within-season irrigation scheduling for maize production in Northwest China: a method based on weather data fusion and yield prediction by DSSAT. Agric. For. Meteorol. 285–286.
Chen, Y., Zhang, Z., Tao, F., 2018. Improving regional winter wheat yield estimation through assimilation of phenology and leaf area index from remote sensing data. Eur. J. Agron. 101, 163–173.
Dawson, I., Wardlaw, I., 1989. The tolerance of wheat to high temperatures during reproductive growth. III. Booting to anthesis. Aust. J. Agric. Res. 40 (5), 965–980.
Donatelli, M., Confalonieri, R., 2011. Biophysical Models For Cropping System simulation, Bio-economic models Applied to Agricultural Systems. Springer, pp. 59–86.
Everingham, Y., Sexton, J., Skocaj, D., Inman-Bamber, G., 2016. Accurate prediction of sugarcane yield using a random forest algorithm. Agron. Sustain. Dev. 36 (2).
Fageria, N.K., 2007. Yield physiology of rice. J. Plant Nutr. 30 (6), 843–879.
Fan, J., Jintrawet, A., Sangchyoswat, C., 2020. The relationships between extreme precipitation and rice and maize yields using machine learning in Sichuan Province, China. Curr. Appl. Sci. 453–469.
FAO, 2017. FAOSTAT. FAO (Accessed 01 June 2019). http://www.fao.org/faostat/en/#home.
FAO, 2018. World Food and Agriculture–Statistical Pocketbook.
Feng, P., et al., 2020. Dynamic wheat yield forecasts are improved by a hybrid approach using a biophysical model and machine learning technique. Agric. For. Meteorol. 285–286.
Feng, P., et al., 2018. Impacts of rainfall extremes on wheat yield in semi-arid cropping systems in eastern Australia. Clim. Change 147 (3–4), 555–569.
Feng, P., Wang, B., Liu, D.L., Yu, Q., 2019. Machine learning-based integration of remotely-sensed drought factors can improve the estimation of agricultural drought in South-Eastern Australia. Agric. Syst. 173, 303–316.
Filippi, P., et al., 2019. An approach to forecast grain crop yield using multi-layered, multi-farm data sets and machine learning. Precis. Agric. 20 (5), 1015–1029.
Folberth, C., et al., 2016. Uncertainty in soil data can outweigh climate impact signals in global crop yield simulations. Nat. Commun. 7 (1), 1–13.
Gao, J., et al., 2019. Effects of climate change on the extension of the potential double cropping region and crop water requirements in Northern China. Agric. For. Meteorol. 268, 146–155.
Gao, Z., et al., 2017. Supplemental irrigation at tasseling optimizes water and nitrogen distribution for high-yield production in spring maize. Field Crop. Res. 209, 120–128.
Grundy, M.J., et al., 2016. Scenarios for Australian agricultural production and land use to 2050. Agric. Syst. 142, 70–83.
Guo, Y., et al., 2020. Integrated phenology and climate in rice yields prediction using machine learning methods. Ecol. Indic. 120, 106935.
Han, J., et al., 2020. Prediction of Winter Wheat Yield Based on Multi-Source Data and Machine Learning in China. Remote Sens. (Basel) 12 (2).
Jeong, J.H., et al., 2016. Random forests for global and regional crop yield predictions. PLoS ONE 11 (6), e0156571.
Jiang, H., et al., 2020. A deep learning approach to conflating heterogeneous geospatial data for corn yield estimation: a case study of the US Corn Belt at the county level. Glob. Chang. Biol. 26 (3), 1754–1766.
Johnson, M.D., Hsieh, W.W., Cannon, A.J., Davidson, A., Bédard, F., 2016. Crop yield forecasting on the Canadian Prairies by remotely sensed vegetation indices and machine learning methods. Agric. For. Meteorol. 218-219, 74–84.
Kouadio, L., Newlands, N., Davidson, A., Zhang, Y., Chipanshi, A., 2014. Assessing the performance of MODIS NDVI and EVI for seasonal crop yield forecasting at the ecodistrict scale. Remote Sens. (Basel) 6 (10), 10193–10214.
Lecerf, R., Ceglar, A., López-Lozano, R., Van Der Velde, M., Baruth, B., 2019. Assessing the information in crop model and meteorological indicators to forecast crop yield over Europe. Agric. Syst. 168, 191–202.
Leroux, L., et al., 2019. Maize yield estimation in West Africa from crop process-induced combinations of multi-domain remote sensing indices. Eur. J. Agron. 108, 11–26.
Li, A., Liang, S., Wang, A., Qin, J., 2007. Estimating crop yield from multi-temporal satellite data using multivariate regression and neural network techniques. Photogramm. Eng. Remote Sens. 73 (10), 1149–1157.
Li, L., et al., 2019a. Future projections of extreme temperature events in different sub-regions of China. Atmos. Res. 217, 150–164.

Li, Q., et al., 2008. Effects of irrigation and planting patterns on radiation use efficiency and yield of winter wheat in North China. Agric. Water Manag. 95 (4), 469–476.
Li, Y., Guan, K., Schnitkey, G.D., DeLucia, E., Peng, B., 2019b. Excessive rainfall leads to maize yield loss of a comparable magnitude to extreme drought in the United States. Glob. Chang. Biol. 25 (7), 2325–2337.
Li, Y., et al., 2019c. Toward building a transparent statistical model for improving crop yield prediction: modeling rainfed corn in the US. Field Crop. Res. 234, 55–65.
Li, Y., et al., 2014. Assimilating remote sensing information into a coupled hydrology-crop growth model to estimate regional maize yield in arid regions. Ecol. Modell. 291, 15–27.
Liu, A., Zhao, S., 2018. High-performance target tracking scheme with low prediction precision requirement in WSNs. Int. J. Ad Hoc Ubiquitous Comput. 29 (4), 270–289.
Liu, H.-l., et al., 2017a. Using the DSSAT model to simulate wheat yield and soil organic carbon under a wheat-maize cropping system in the North China Plain. J. Integr. Agric. 16 (10), 2300–2307.
Liu, L., Gao, Y., Liu, X., 2019. High-dimensional vortex beam encoding/decoding for high-speed free-space optical communication. Opt. Commun. 452, 40–47.
Liu, X., et al., 2017b. Using an active-optical sensor to develop an optimal NDVI Dynamic model for high-yield rice production (Yangtze, China). Sens. (Basel) 17 (4).
Lobell, D.B., Field, C.B., 2007. Global scale climate–crop yield relationships and the impacts of recent warming. Environ. Res. Lett. 2 (1).
Maya Gopal, P.S., Bhargavi, R., 2019. Performance Evaluation of Best Feature Subsets for Crop Yield Prediction Using Machine Learning Algorithms. Appl. Artif. Intell. 33 (7), 621–642.
Meng, W., Tao, F., Shi, W., 2014. Corn yield forecasting in northeast china using remotely sensed spectral indices and crop phenology metrics. J. Integr. Agric. 13 (7), 1538–1545.
Mkhabela, M.S., Bullock, P., Raj, S., Wang, S., Yang, Y., 2011. Crop yield forecasting on the Canadian Prairies using MODIS NDVI data. Agric. For. Meteorol. 151 (3), 385–393.
Moldenhauer, K., Slaton, N., 2001. Rice growth and development. Rice Prod. Handb. 192, 7–14.
Molinaro, A.M., Simon, R., Pfeiffer, R.M., 2005. Prediction error estimation: a comparison of resampling methods. Bioinformatics 21 (15), 3301–3307.
Mu, H., et al., 2010. Long-term low radiation decreases leaf photosynthesis, photochemical efficiency and grain yield in winter wheat. J. Agron. Crop Sci. 196 (1), 38–47.
Nandram, B., Berg, E., Barboza, W., 2013. A hierarchical Bayesian model for forecasting state-level corn yield. Environ. Ecol. Stat. 21 (3), 507–530.
Otteson, B.N., Mergoum, M., Ransom, J., Schatz, B., 2008. Tiller contribution to spring wheat yield under varying seeding and nitrogen management. Agron. J. 100 (2), 406–413.
Palosuo, T., et al., 2011. Simulation of winter wheat yield and its variability in different climates of Europe: a comparison of eight crop growth models. Eur. J. Agron. 35 (3), 103–114.
Peng, B., et al., 2020. Assessing the benefit of satellite-based Solar-Induced Chlorophyll Fluorescence in crop yield prediction. Int. J. Appl. Earth Obs. Geoinform. 90.
Piao, S., et al., 2010. The impacts of climate change on water resources and agriculture in China. Nature 467 (7311), 43–51.
Puig, E., Gonzalez, F., Hamilton, G., Grundy, P., 2015. Assessment of Crop Insect Damage Using Unmanned Aerial systems: A machine Learning Approach.
Rossato, L., et al., 2017. Impact of soil moisture on crop yields over Brazilian semiarid. Front. Environ. Sci. 5.
Royo, C., et al., 2006. Grain growth and yield formation of durum wheat grown at contrasting latitudes and water regimes in a Mediterranean environment. Cereal Res. Commun. 34 (2–3), 1021–1028.
Schwalbert, R.A., et al., 2020. Satellite-based soybean yield forecast: integrating machine learning and weather data for improving crop yield prediction in southern Brazil. Agric. For. Meteorol. 284.
Shahhosseini, M., Hu, G., Huber, I., Archontoulis, S.V., 2021. Coupling machine learning and crop modeling improves crop yield prediction in the US Corn Belt. Sci Rep 11 (1), 1606.
Silvestro, P., et al., 2017. Estimating wheat yield in China at the field and district scale from the assimilation of satellite data into the aquacrop and Simple Algorithm for Yield (SAFY) models. Remote Sens. (Basel) 9 (5).
Singh, B., Reddy, K.R., Redoña, E.D., Walker, T., 2017. Screening of rice cultivars for morpho-physiological responses to early-season soil moisture stress. Rice Sci. 24 (6), 322–335.
Singh, R.P., Prasad, A.K., Tare, V., Kafatos, M., 2010. Crop yield prediction using piecewise linear regression with a break point and weather and agricultural parameters. Google Pat.
Soltani, A., 2012. Modeling Physiology of Crop development, Growth and Yield. CABi.
Son, N., Chen, C., Chen, C., Minh, V., Trung, N., 2014. A comparative analysis of multitemporal MODIS EVI and NDVI data for large-scale rice yield estimation. Agric. For. Meteorol. 197, 52–64.
Sonobe, R., Tani, H., Wang, X., Kobayashi, N., Shimamura, H., 2014. Random forest classification of crop type using multi-temporal TerraSAR-X dual-polarimetric data. Remote Sens. Lett. 5 (2), 157–164.
Stefan, J., 2018. Hands-On Machine Learning For Algorithmic Trading. Packt Publishing.
Stephenson, N., 1998. Actual evapotranspiration and deficit: biologically meaningful correlates of vegetation distribution across spatial scales. J. Biogeogr. 25 (5), 855–870.
Sui, B., et al., 2013. Optimizing nitrogen supply increases rice yield and nitrogen use efficiency by regulating yield formation factors. Field Crop. Res. 150, 99–107.
Tao, F., Yokozawa, M., Liu, J., Zhang, Z., 2008. Climate–crop yield relationships at provincial scales in China and the impacts of recent climate trends. Clim. Res. 38, 83–94.
Thorp, K., et al., 2012. Estimating crop biophysical properties from remote sensing data by inverting linked radiative transfer and ecophysiological models. Remote Sens. Environ. 124, 224–233.
Tilman, D., Balzer, C., Hill, J., Befort, B.L., 2011. Global food demand and the sustainable intensification of agriculture. Proc Natl Acad Sci U S A 108 (50), 20260–20264.
Vicente-Serrano, S.M., Beguería, S., López-Moreno, J.I., 2010. A multiscalar drought index sensitive to global warming: the standardized precipitation evapotranspiration index. J. Clim. 23 (7), 1696–1718.
Wang, B., et al., 2018. Estimating soil organic carbon stocks using different modelling techniques in the semi-arid rangelands of eastern Australia. Ecol. Indic. 88 (MAY), 425–438.
Wang, H., et al., 2016. Monitoring winter wheat drought threat in Northern China using multiple climate-based drought indices and soil moisture during 2000–2013. Agric. For. Meteorol. 228, 1–12.
Wang, J., et al., 2020. Integrating remote sensing-based process model with environmental zonation scheme to estimate rice yield gap in Northeast China. Field Crop. Res. 246, 107682.
Wei, T., Cherry, T.L., Glomrod, S., Zhang, T., 2014. Climate change impacts on crop yield: evidence from China. Sci. Total Environ. 499, 133–140.
Whish, J.P., Herrmann, N.I., White, N.A., Moore, A.D., Kriticos, D.J., 2015. Integrating pest population models with biophysical crop models to better represent the farming system. Environ. Modell. Softw. 72, 418–425.
Wickham, H., 2011. ggplot2, 3. Wiley Interdisciplinary Reviews: Computational Statistics, pp. 180–185.
Wu, B., et al., 2013. Remote sensing-based global crop monitoring: experiences with China's CropWatch system. Int. J. Digit. Earth 7 (2), 113–137.
Xiao, D., Liu, D.L., Wang, B., Feng, P., Waters, C., 2020. Designing high-yielding maize ideotypes to adapt changing climate in the North China Plain. Agric. Syst. 181.
Xie, Y., et al., 2017. Assimilation of the leaf area index and vegetation temperature condition index for winter wheat yield estimation using Landsat imagery and the CERES-Wheat model. Agric. For. Meteorol. 246, 194–206.
Yang, X., et al., 2015. Potential benefits of climate change for crop productivity in China. Agric. For. Meteorol. 208, 76–84.
Yao, N., Li, Y., Lei, T., Peng, L., 2018. Drought evolution, severity and trends in mainland China over 1961–2013. Sci. Total Environ. 616-617, 73–89.
Zhang, J., Chen, Y., Zhang, Z., 2020a. A remote sensing-based scheme to improve regional crop model calibration at sub-model component level. Agric. Syst. 181.
Zhang, Y., Song, B., Zhang, Y., Chen, S., 2017. An advanced random forest algorithm targeting the big data with redundant features. In: International Conference on Algorithms and Architectures for Parallel Processing. Springer, pp. 642–651.
Zhang, Z., Li, Z., Chen, Y., Zhang, L., Tao, F., 2020b. Improving regional wheat yields estimations by multi-step-assimilating of a crop model with multi-source data. Agric. For. Meteorol. 290.
Zhao, S., 1983. A new scheme for comprehensive physical regionalization in China. Acta Geograph. 38 (1), 1–10.
Zhao, Y., Chen, S., Shen, S., 2013. Assimilating remote sensing information with crop model using Ensemble Kalman Filter for improving LAI monitoring and yield estimation. Ecol. Modell. 270, 30–42.